

See discussions, stats, and author profiles for this publication at: <https://www.researchgate.net/publication/268793136>

Nanoparticulate Coatings with Efficient Up-Conversion Properties

ARTICLE *in* ACS APPLIED MATERIALS & INTERFACES · NOVEMBER 2014

Impact Factor: 6.72 · DOI: 10.1021/am5065377 · Source: PubMed

READS

69

5 AUTHORS, INCLUDING:



Geraldine Dantelle

Institut Néel

58 PUBLICATIONS 880 CITATIONS

[SEE PROFILE](#)



Carlos Zaldo

Spanish National Research Council

242 PUBLICATIONS 3,510 CITATIONS

[SEE PROFILE](#)



Concepción Cascales

Spanish National Research Council

212 PUBLICATIONS 2,533 CITATIONS

[SEE PROFILE](#)



Thierry Gacoin

French National Centre for Scientific Research

215 PUBLICATIONS 5,754 CITATIONS

[SEE PROFILE](#)

Nanoparticulate Coatings with Efficient Up-Conversion Properties

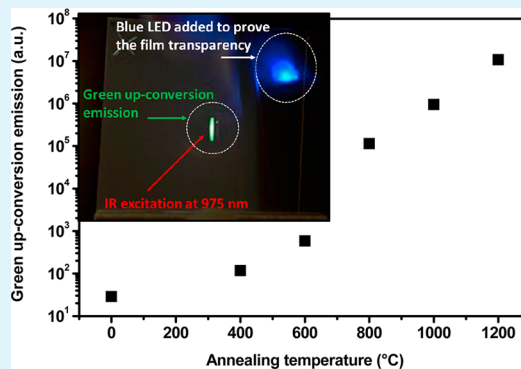
Geraldine Dantelle,^{*,†,§} Rocío Calderón-Villajos,[‡] Carlos Zaldo,[‡] Concepción Cascales,[‡] and Thierry Gacoin[†]

[†]Laboratoire de Physique de la Matière Condensée, Ecole Polytechnique, CNRS UMR 7643 Route de Saclay, 91 128 Palaiseau Cedex, France

[‡]Instituto de Ciencia de Materiales de Madrid, Consejo Superior de Investigaciones Científicas c/Sor Juana Inés de la Cruz 3, Cantoblanco, E-28049 Madrid, Spain

S Supporting Information

ABSTRACT: Nanoparticulate films with high up-conversion emission (UC) properties were prepared by spray-deposition of nanometer-sized YVO₄:Yb,Er particles. The optical properties of YVO₄:Yb,Er were optimized upon annealing before the film deposition in order to get the highest possible UC signal in the considered type of system. Thanks to a simple model and some time-resolved spectroscopic investigations, the contribution of the scattering to the UC signal could be separated from the intrinsic properties (crystallinity, surface defects) of the material. The films obtained by this technique present the advantages of having both high UC and good transparency.



KEYWORDS: up-conversion, rare-earth, films, scattering, YVO₄

1. INTRODUCTION

Up-conversion (UC) mechanism consists of converting two (or more) photons of low energy into one photon of higher energy. Typically, two near-infrared photons are absorbed, and a visible photon is emitted. Since its discovery,¹ UC has been widely studied in bulk materials doped with lanthanide ions for the development of many different applications (lasers,^{2,3} white light production,⁴ etc.). More recently, investigations have been devoted to the study of UC in nano-objects with the main motivation of using them as luminescent probes in biological imaging⁵ and to take benefit from both an excitation in a spectral region where radiations are less absorbed by tissues and a better z-resolution thanks to the quadratic nature of the process.⁶ Another application of UC nanoemitters could be envisioned to elaborate transparent UC emitting devices for the photovoltaic applications^{7,8} or for the development of head-up displays⁹ or full-color UC displays. The dispersion of nanopowders in a nanostructured transparent polymeric matrix¹⁰ or the formation of nanocrystals embedded inside a glassy matrix and forming glass-ceramics^{11–13} are currently proposed for these purposes. However, the dilution of the nanoemitters within a matrix reduces the overall emitted UC signal. Elaborating coatings exclusively made of UC emitting nanocrystals appears to be a real challenge with respect to the optical and mechanical quality.

Regarding bulk materials, it is well-known that fluoride compounds present higher UC quantum yield than oxides because of their reduced phonon energy.¹⁴ At the nanoscale,

the matrix phonon does not seem to be the limiting parameter for UC efficiency when considering nonradiative de-excitations from surface and volume defects.¹⁵ Indeed, observing efficient UC emission in nanoparticles is particularly tricky because the small particle size induces a close proximity between lanthanide ions and the surface where a large amount of quenching species (hydroxyl or organic groups) are present, shortening excited level lifetimes and thus reducing the UC efficiency. A large number of studies have thus been devoted to producing structured core/shell nanoparticles to minimize the effects of surface traps.^{16–19} In addition, the volume defects in nanoparticles are also strong channels for nonradiative de-excitations, as we recently showed through the study of the optical properties of 40 nm YVO₄:Yb,Er nanoparticles.¹⁵ Nevertheless, the relatively low temperatures of synthesis required to elaborate nanosized particles, as compared to bulk compounds, lead to a limited control of particle crystallinity and thus to the presence of crystalline defects that also limit UC efficiency. In our previous work,¹⁵ we showed that ultimate improvement of the particle crystallinity allows oxide nanoparticles of YVO₄:Yb,Er to exhibit emission properties comparable to those exhibited by fluoride nanoparticles.¹⁵ We concluded that the disadvantage of oxides in terms of phonon energy can be compensated with the ability to obtain particles

Received: September 23, 2014

Accepted: November 19, 2014

Published: November 19, 2014

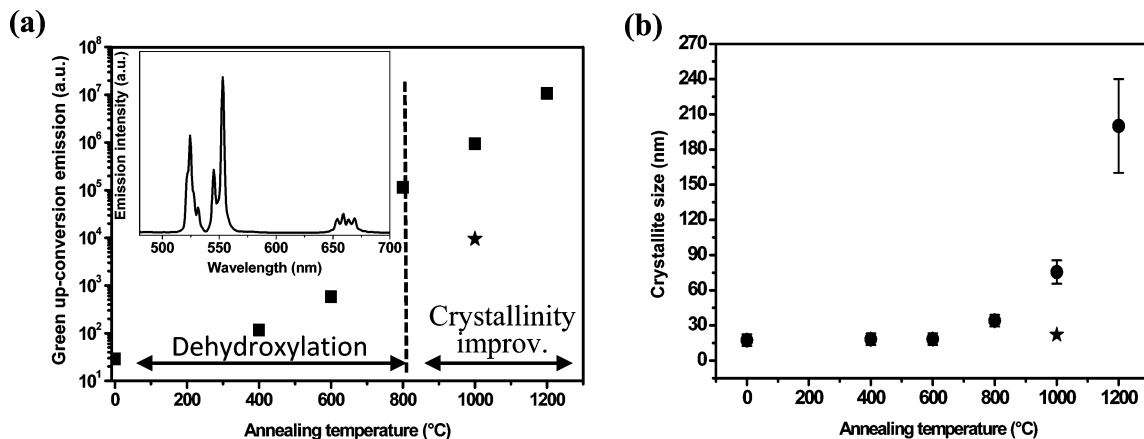


Figure 1. (a) Evolution of the UC intensity of YVO₄:20%Yb,2%Er as a function of the annealing temperature (■), under a 975 nm excitation of about 100 W·cm⁻². For comparison, measurements were done on YVO₄ powders incorporated into KBr pellets. Note that the y axis in log scale; (inset) a typical UC spectrum of YVO₄:20%Yb,2%Er. (b) Evolution of the crystallite size of YVO₄:Yb,Er upon annealing temperature. In both graphs, the star (★) corresponds to a YVO₄:20%Yb,2%Er sample that has been annealed at 1000 °C in silica (protected annealing). For the measurements, the silica has been removed.

with a better crystallinity than fluorides. In addition, oxides present a better chemical stability and an easier functionalization for aqueous dispersion as compared to fluorides. All this provides strong motivation to keep considering oxides as good candidates as UC nanoemitters.

The strategy developed in our group for elaborating highly efficient UC nanoemitters consists of first synthesizing the nanoparticles by aqueous coprecipitation at room temperature and then annealing them at high temperature in a matrix to avoid their sintering and increase their crystallinity.²⁰ This “protected annealing” strategy has appeared to be very efficient, leading to oxide particles with ultimate emission properties. This process nevertheless presents some drawbacks, mainly because it is time-consuming and hazardous, thus only allowing the production of particles in small quantities. Although it is not restrictive for biological labeling applications, this drawback is a severe limitation in the context of UC emitting coatings because the weak absorption cross-section of lanthanide ions requires the elaboration of relatively thick (typically of a few microns or more) films to get enough UC signal.

Some physical methods, such as the pulsed laser deposition technique,²¹ can successfully produce UC emitting films; however, the film thickness is limited, and these techniques are often time-consuming, expensive, and limited to small substrates. In this study, we present a method based on spray-deposition of YVO₄:Yb,Er particles to prepare transparent UC emitting coatings that are scalable on large dimensions and over flexible substrates. We focus our work on the possibility to get high UC intensity and a controlled transparency of the coatings. With the aim of obtaining the highest UC intensity, we also address the problem of comparing UC efficiency of powder samples, showing that it is often biased by scattering effects.

2. EXPERIMENTAL SECTION

2.1. Synthesis of YVO₄:Yb,Er. YVO₄ nanoparticles doped with 2 mol % Er³⁺ and 20 mol % Yb³⁺ ions have been synthesized by room-temperature coprecipitation according to a previously reported method.¹⁵ Briefly, 15.6 mL of Y(NO₃)₃ (0.1M), 4 mL of Yb(NO₃)₃ (0.1 M), and 0.4 mL of Er(NO₃)₃ (0.1 M) were slowly added to 20 mL of Na₃VO₄ (*c* = 0.1 M) at room temperature under vigorous stirring. After a 30 min reaction time, the precipitate was purified by

successive centrifugations and washings in water (three times, at 11 000 rpm for 15 min). The obtained solution consists of Y_{0.78}Yb_{0.2}Er_{0.02}VO₄ nanoparticles dispersed in water. These nanoparticles, labeled YVO₄:Yb,Er in the following, were dried in an oven and annealed at different temperatures (400–1200 °C with a 5 °C/min ramp) for 10 h.

To compare UC efficiency on powder samples, we mixed a small amount of the obtained powders (10 mg) with KBr (150 mg) and pressed the mixtures to form dense pellets (pressure, 50 kN).

The powders, annealed at 800 and 1200 °C, aggregated, and partially sintered, were ground using a planetary mill to reduce the aggregate size. Typically, 300 mg of powder was mixed with 30 mL of diethylene glycol in the milling bowl, which was then shaken at 450 rpm for 10 min. After a 5 min break to evacuate heat, the process was repeated four times. The resulting mixture was then inserted into centrifugation tubes and the solid content was retrieved after a 40 min centrifugation at 11 000 rpm. Two additional ethanol washings were performed (11 000 rpm; i.e., g-force = 11 353, 30 min) to finally obtain particles in suspension in ethanol, which is perfectly appropriate for the elaboration of coatings by spray-deposition, as explained hereafter. The whole synthesis process is illustrated on Figure S1 (Supporting Information).

Non annealed YVO₄:Yb,Er nanoparticles were encapsulated into a SiO₂ sol–gel matrix before a thermal treatment. This process enables high-temperature annealing treatment without inducing particle sintering. This process is called “protected annealing”. A silica sol was prepared by mixing 5 mL of triethoxyorthosilicate, 5 mL of ethanol, and 2.05 mL of water at pH 1.25. The mixture was heated at 60 °C under reflux for 1 h. YVO₄:Yb,Er nanoparticles were dispersed into the silica solution with a dispersing agent (PE6800) in the molar proportion Y/Si/PE6800 = 1:5:0.05 and dried in an oven until total evaporation of the solvent was achieved. The composite powder was then annealed at 1000 °C for 10 h. After annealing, the nanoparticles encapsulated into the silica matrix can be retrieved by dissolving the silica matrix in a HF solution (5%), as previously reported.²²

2.2. Preparation of YVO₄:Yb,Er Coatings. Nanoparticulate coatings were prepared using spray-deposition.²³ Briefly, YVO₄:Yb,Er particles in ethanolic solutions (*c* ~ 2 g/L) were put in a Paasche Talon airbrush and sprayed onto 1 × 1 in., 1 mm thick microscope slides. These substrates were previously heated at 60 °C, close to the evaporation temperature of ethanol, which allows the formation of homogeneous coatings and avoids solution dripping.

2.3. Structural and Optical Characterizations of YVO₄:Yb,Er Particles and Coatings. Powder X-ray diffraction (XRD) patterns were measured on a Philips X'Pert instrument with a Cu K α cathode. They enable the determination of the material phase and the crystallite

size from the full-width half-maximum (fwhm) of the diffraction peaks. Particle size and particle and film morphology were investigated by scanning electron microscopy (FEG-SEM Hitachi 4800). Particles were also observed by transmission electron microscopy (TEM; Philips CM 30).

$\text{YVO}_4\text{:Yb,Er}$ powders in KBr pellets were excited at 975 nm using a 1 W laser diode (L97SP1WJ Thorlabs) and their UC emission was detected with an Ocean Optics spectrometer (QE 65 000). To compare the efficiency of the different samples, green and red emissions were integrated between 500 and 600 nm and 600 and 700 nm, respectively, and normalized in acquisition time. Time-resolved experiments were performed on powder samples using a short (<10 ns) pulsed laser MOPA system at 979 nm and measured with different photomultipliers at 1050 or 550 nm. The effective lifetimes of the $^2\text{F}_{5/2}$ level of Yb^{3+} and $^4\text{S}_{3/2}$ level of Er^{3+} were calculated using the following formula:

$$\tau = \frac{\int_0^\infty t \times I(t)}{\int_0^\infty I(t)}$$

Direct transmission measurements of the different coatings were performed on an absorption spectrometer (Cary 50). Further measurements were performed using BYK Gardner haze-gard plus equipment, enabling us to measure the percentage of total transmitted light through the films, the haze corresponding to the wide-angle scattering (i.e., the percentage of light transmitted in the $0\text{--}87.5^\circ$ and $92.5\text{--}180^\circ$ light cones), and the clarity corresponding to the narrow angle-scattering, (i.e., the percentage of light that is deviated from less than 0.1° from the axis of the incident light when the light passes through the sample). Emission intensity of $\text{YVO}_4\text{:Yb,Er}$ coatings was recorded on the same optical bench as $\text{YVO}_4\text{:Yb,Er}$ powders.

3. RESULTS AND DISCUSSION

3.1. Evolution of the $\text{YVO}_4\text{:Yb,Er}$ UC Intensity upon Annealing Temperature. **3.1.1. Experimental Results.** The up-conversion emission of $\text{YVO}_4\text{:Yb,Er}$ particles was studied under a 975 nm excitation. The emission spectrum (Figure 1a, inset) is characteristic of a Yb–Er system with bands centered at 520 nm, 550 and 660 nm corresponding to the $^2\text{H}_{11/2} \rightarrow ^4\text{I}_{15/2}$, $^4\text{S}_{3/2} \rightarrow ^4\text{I}_{15/2}$ and $^4\text{F}_{9/2} \rightarrow ^4\text{I}_{15/2}$ of Er^{3+} respectively. Intensities of both green and red up-conversion emissions drastically increase with the increase of the annealing temperature, as shown in Figure 1a and Figure S2 (Supporting Information). Note that the y axis is in log scale. This evolution is well-known^{24,25} and can be explained, at least partially, by the removal of hydroxyl surface groups that are particularly detrimental for UC, as these groups have high phonon energies (e.g., $\sim 3300 \text{ cm}^{-1}$ for $-\text{OH}$), favoring nonradiative pathways. Indeed up-conversion processes are very sensitive to nonradiative relaxations, which hinder efficient energy transfers between Yb and Er ions by shortening lifetime of intermediate states involved in the UC process, thus preventing high UC. However, the UC intensity continues to increase very significantly for annealing temperatures above 800°C , a temperature over which almost no organic group should remain. Other parameters should thus be taken into account to explain this increase of luminescence.

Through the Scherrer's analyses of X-ray diffraction patterns of $\text{YVO}_4\text{:Yb,Er}$ upon annealing, the average crystallite size was determined: it strongly increases with the annealing temperature (Figure 1b), showing the increase of the particle crystallinity. This enlargement implies a reduction of volume defects and thus favors the UC emission by limiting the nonradiative de-excitations. In addition to crystallite growth, there is also particle growth, which modifies the scattering rate

within the sample by artificially increasing the excitation rate and modifying the collected UC. Finally, the particle growth may also influence the radiative de-excitation rate as it modifies the average refractive index nearby the emitters and thus modifies the radiative lifetime. Indeed, the influence of the surrounding dielectric medium on the fluorescence lifetime of rare-earth-doped materials has already been discussed in the literature. The first report in the literature was done in 1999 by Meltzer et al., who published that the radiative lifetime of Eu^{3+} in Y_2O_3 10 nm particles was 4 times longer than in the corresponding bulk material due to the change of refractive index of the surrounding medium.²⁶ More recently, Vetrone et al. showed a lengthening of the $^4\text{S}_{3/2}$ and $^4\text{F}_{9/2}$ level lifetime of Er^{3+} in Lu_2O_3 50 nm nanoparticles compared to bulk material.²⁷ Regarding the 40 nm YVO_4 nanoparticles, this effect has been highlighted when the compound is doped with Eu^{3+} ions.^{20,28,29}

As a summary, different factors may contribute to the increase of the UC intensity with the annealing temperature in the $0\text{--}1200^\circ\text{C}$ temperature range: (1) the reduction of nonradiative de-excitations because of the removal of surface and volume traps (2) the scattering, associated with the particle growth and (3) the effect of the dielectric medium through the increase of the effective refractive index associated with the particles growth, affecting radiative recombination rates.

In order to prepare transparent $\text{YVO}_4\text{:Yb,Er}$ coatings with the highest UC, it is necessary to understand how the different contributions influence the UC efficiency. To separate the contributions (those due to intrinsic properties of $\text{YVO}_4\text{:Yb,Er}$ particles and those due to the scattering), the Yb–Er system was modeled, and additional experiments, including time-resolved spectroscopy, were performed.

3.1.2. Presentation of the Model. According to the model described in ref 30 and the energy level diagram described in Figure S4 (Supporting Information), the following population equations can be written:

$$\frac{dN_{\text{Yb}1}}{dt} = \sigma\rho N_{\text{Yb}0} - \frac{N_{\text{Yb}1}}{\tau_{\text{Yb}}} \quad (1)$$

$$\frac{dN_1}{dt} = C_0 N_0 N_{\text{Yb}1} - C_1 N_1 N_{\text{Yb}1} - \frac{N_1}{\tau_1} \quad (2)$$

$$\frac{dN_2}{dt} = C_1 N_1 N_{\text{Yb}1} - \frac{N_2}{\tau_2} \quad (3)$$

where σ is the absorption cross-section of Yb^{3+} , ρ is the excitation photon flux, τ_{Yb} is the $^2\text{F}_{5/2}$ level lifetime of Yb^{3+} , τ_1 is the $^4\text{I}_{13/2}$ level lifetime of Er^{3+} , and τ_2 is the $^4\text{S}_{3/2}$ level lifetime of Er^{3+} .

In this model, we hypothesize that $N_{\text{Yb}1}$ is depleted only by the linear rate ($^2\text{F}_{5/2} \rightarrow ^2\text{F}_{7/2}$) and that the depletion due to the ETU transfers is neglected. This can be justified by looking at the emission spectra in the NIR and visible ranges (Figure S3, Supporting Information). The emission corresponding to the $^2\text{F}_{5/2} \rightarrow ^2\text{F}_{7/2}$ transition of Yb^{3+} dominates the spectra for both micro- and nanosized particles. According to this model, in the steady-state regime and at high excitation intensity, the UC intensity can be written as

$$I = C_0 N_0 N_{\text{Yb}0} \sigma \rho h\nu \left(\frac{\tau_2}{\tau_{\text{rad}}} \right) \tau_{\text{Yb}} \quad (4)$$

The values of τ_2 and τ_{Yb} have been measured as a function of the annealing temperature and are reported in Figure 2. Some of the fluorescence decays are also presented in Figure S5 (Supporting Information).

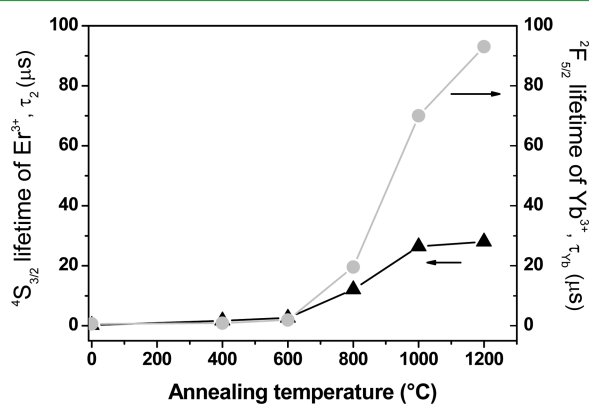


Figure 2. Evolution of annealing temperatures of ${}^4\text{S}_{3/2}$ Er^{3+} and ${}^5\text{F}_{5/2}$ Yb^{3+} lifetimes in $\text{YVO}_4:\text{Yb},\text{Er}$ powders under a 975 nm excitation.

τ_2^{rad} is given by the expression $(1/(\tau^{\text{rad}})) = ((f(ED)(\lambda_0^2))/(n(n^2 + 2)^2))$ where n is the refractive index of the dielectric medium surrounding the emitters. According to our previous study on YVO_4 nanoparticles,^{22,28,29} the radiative lifetime in $\text{YVO}_4:\text{Yb},\text{Er}$ nanoparticles is affected by the dielectric environment. Consequently, as the measurements are performed on YVO_4 powders embedded into pressed KBr pellets, the considered refractive index is $n = n_{\text{KBr}} = 1.56$ for nanoparticles and $n = n_{\text{YVO}_4} = 2$ for micron-sized particles.

Note that this expression (eq 4) does not take into account the scattering of emitted light. The UC intensity, which is effectively collected onto the detector, corresponds to eq 5:

$$\text{IC} = I \times S_e \quad (5)$$

where S_e corresponds to the scattering rate of the emitted light.

3.1.3. Determination of the Weight of the Different Contributions. To determine the influence of the $\text{YVO}_4:\text{Yb},\text{Er}$ intrinsic properties and of the scattering on the UC intensity, we compared samples annealed at different temperatures. In addition, we compared $\text{YVO}_4:\text{Yb},\text{Er}$ nanoparticles annealed at 1000 °C in a protective silica matrix, which enabled us to have a sample that had undergone a thermal annealing but whose particle size remained small, limiting the scattering effect. The emission intensity and crystallite size of this sample are reported as stars (★) in Figure 1.

An UC intensity ratio of 100 was found experimentally between two samples annealed at 1000 °C, one classically (labeled IC_{1000}) and one annealed in silica (IC_{1000}' ; Table 1). Note that the main difference between the two samples is the crystallite size, related to the difference of particle size.¹⁵ To explain this intensity difference, we calculated the expected value using (eq 4). Details of the calculation are given in section S6 of the Supporting Information. Briefly, considering that the two samples only differ by their grain size, the model allows us to calculate the ratio of scattered (incident and emitted) light between the two samples, corresponding to a factor of 30. As the UC intensity ratio is experimentally of 100, we deduce that there are some intrinsic differences between the particles annealed at 1000 °C and those annealed at 1000 °C in the silica matrix that are responsible for a variation by a factor of ~3.3

Table 1. Structural and Spectroscopic Data of Some $\text{YVO}_4:\text{Yb},\text{Er}$ Compounds That Have Been Annealed under Different Conditions

	crystallite size	τ_{Yb} (μs)	τ_2 (μs)	IC^a
$\text{YVO}_4:\text{Yb},\text{Er}$ annealed at 600 °C	18 nm	1.9	2.6	$\text{IC}_{600} = \text{IC}_{1000}/1750$
$\text{YVO}_4:\text{Yb},\text{Er}$ annealed at 1000 °C	82 nm	70	26.4	IC_{1000}
$\text{YVO}_4:\text{Yb},\text{Er}$ annealed at 1000 °C in silica—silica removed with HF	22 nm	26	8.9	$\text{IC}_{1000}' = \text{IC}_{1000}/100$

^aCollected up-conversion intensity.

(=100/30) of the UC intensity. This factor of 3.3 may correspond to remaining defects at the surface of the nanoparticles.

Similarly, the UC intensity ratio between one sample annealed at 1000 °C (IC_{1000}) and one annealed at 600 °C (IC_{600}) can be measured experimentally (~1750; Table 1). This comparison enables us to determine the contribution of the scattering (see sections S7 and S8, Supporting Information). In this case, the scattering of the excited and emitted light contributes to a factor of 28 at the UC intensity. We deduce that the change of microstructure (improved crystallinity and a reduction of surface and volume defects) between an annealing at 600 °C and an annealing at 1000 °C contributes to an increase of the UC by a factor of $1750/28 = 62.5$.

These comparisons show that an annealing treatment drastically increases the UC efficiency as it is often reported, but the contribution of the scattering effect due to particle growth, rarely mentioned in the literature, should not be minimized. These results are in accordance with the recent study on $\text{NaYF}_4:\text{Yb},\text{Er}$ published by Dyck et al., who show the existence of an optimal annealing temperature to get strong UC intensity while maintaining particle shape.³¹

The method we developed allows the quantification of contributions of both microstructure and scattering and the full understanding of the evolution of the UC intensity of $\text{YVO}_4:\text{Yb},\text{Er}$ upon annealing.

3.2. $\text{YVO}_4:\text{Yb},\text{Er}$ Up-Conversion Emitting Coatings.

3.2.1. Coating Preparation. In light of the above study, thermal annealing of $\text{YVO}_4:\text{Yb},\text{Er}$ nanoparticles synthesized by coprecipitation is necessary in order to get highly efficient UC emitting coatings. As the final goal is to obtain coatings with controlled transparency, the size of $\text{YVO}_4:\text{Yb},\text{Er}$ particles should remain at the nanometer scale. One possibility could be to apply our protected annealing process¹⁵ and then deposit the particles; nevertheless, we focused on another strategy that proved to be simpler and thus allowed for higher mass production. The basic principle relies on the thermal annealing of nanoparticles powder and the reduction of agglomerate sizes by mechanical grind.

According to the UC intensity values reported in Figure 1, we chose two samples: one annealed at 800 °C and the other annealed at 1200 °C. The mechanical grinding was performed in a liquid environment to minimize aggregation. After successive washings by centrifugation, the particles were retrieved in ethanol. SEM and TEM images of both types of particles were taken, as illustrated in Figure 3.

The nanoparticles resulting from an annealing at 800 °C followed by a mechanical grinding (labeled P800G) are aggregated, but the individual 40 nm starting nanoparticles

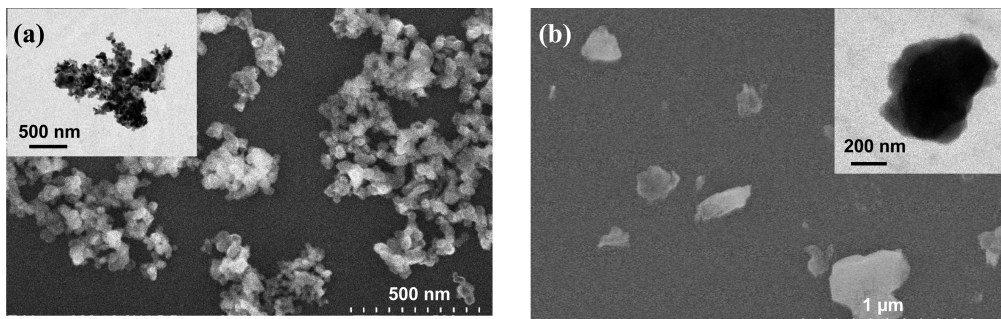


Figure 3. SEM images of $\text{YVO}_4:\text{Yb},\text{Er}$ particles resulting from (a) thermal annealing at $800\text{ }^\circ\text{C}$ for 10 h and a grinding and (b) thermal annealing at $1200\text{ }^\circ\text{C}$ for 10 h and a grinding. (Insets) TEM images of the corresponding particles.

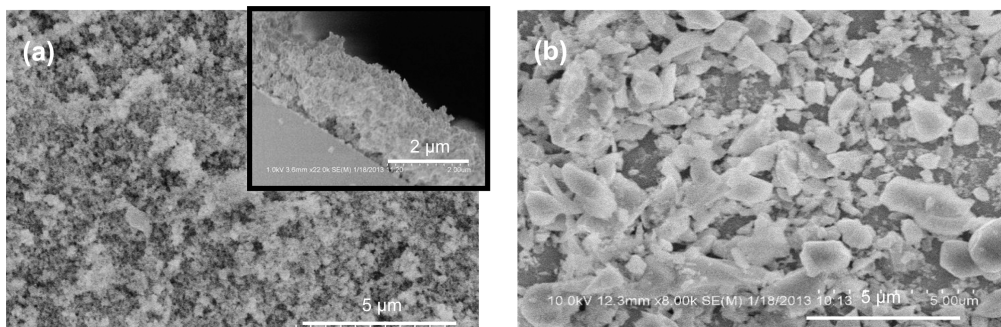


Figure 4. SEM images of coatings obtained by the spray-deposition (a) of $\text{YVO}_4:\text{Yb},\text{Er}$ particles after a thermal annealing at $800\text{ }^\circ\text{C}$ and a mechanical grinding and (b) of $\text{YVO}_4:\text{Yb},\text{Er}$ particles after a thermal annealing at $1200\text{ }^\circ\text{C}$ and a mechanical grinding. (a, inset) Cross-sectional image of the film. The film thickness is measured to be $\sim 2\text{ }\mu\text{m}$.

can be still distinguished. At the opposite, the nanoparticles resulting from an annealing at $1200\text{ }^\circ\text{C}$ followed by a mechanical grinding (labeled P1200G) do not present any microstructure. The sintering is complete, and the morphology of the initial particles has completely disappeared.

Particle coatings onto glass substrates were elaborated by spray-depositing 2 mL of colloidal solutions containing either P800G particle or P1200G particle solutions ($c \sim 2\text{ g/L}$). Their morphology has been studied by SEM (Figure 4).

A much more homogeneous surface coverage is obtained when the P800G particles are used compared to that of P1200G particles. The cross-section of the film made from P800G particles reveals a relatively homogeneous thickness ($\sim 2\text{ }\mu\text{m}$), as illustrated in the inset of Figure 4a. This difference of film morphology arises from the fact that the same quantity of matter is deposited, but because the P1200G particles are bigger, the film is incomplete and rougher. Moreover, the difference can be explained by the likely mobility of the P800G particles that are composed of aggregates of nanoparticles. The rearrangement of these units seems possible during the spray-deposition and the drying phase. This explanation is reinforced by the study of single drop spraying (Figure S9, Supporting Information) which reveals that the solution made of P800G behaves like a colloidal solution of nanoparticles, forming rings when reaching the substrate.²³

Qualitatively, the mechanical properties of the film made of P800G particles, and especially the particle adhesion onto the glass substrate, appear greatly improved as compared to those of the film made of P1200G particles. Note that spraying non annealed nanoparticles and performing a thermal treatment after the deposition is not an appropriate choice as we face cracks and problems with the substrate thermal resistance.

3.2.2. Film Optical Properties. The absorption spectra of the films obtained by spraying 2 mL of either P800G particles or P1200G particles are presented in Figure 5. The transmission

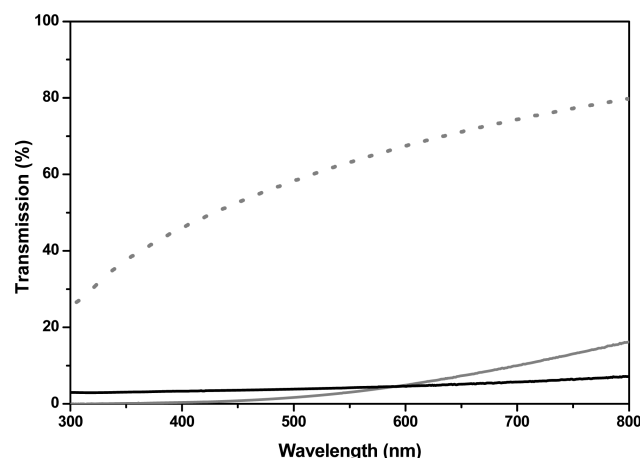


Figure 5. Transmission spectra of films made by spraying (black solid line) 2 mL of P1200G nanoparticles, (gray solid line) 2 mL of P800G particles, and (gray dotted line) 0.5 mL of P800G particles.

spectra look different between these two samples, probably due to different scattering regimes linked to the different surface coverage of the samples. One can note that, although the film made of P1200G particles does not present a complete surface coverage, its transparency is lower (7% at 800 nm) than the film made with the same quantity of P800G particles (16% at 800 nm).

On the same graph (Figure 5) is added the absorption spectrum of a film corresponding to the spray-deposition of 0.5

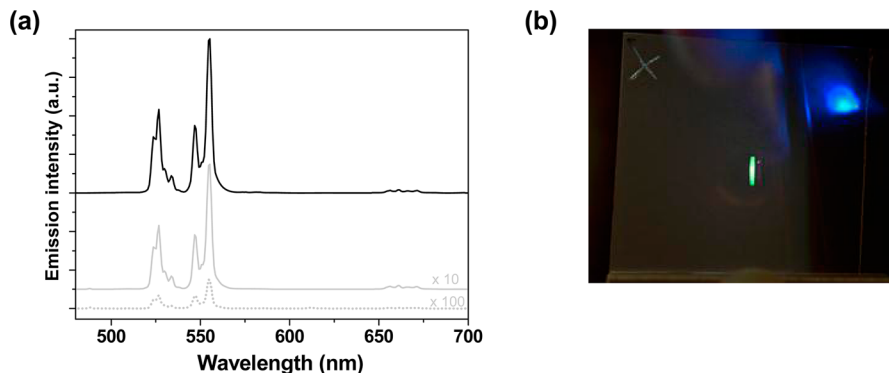


Figure 6. (a) UC emission spectra of $\text{Yb},\text{Er}:\text{YVO}_4$ films made by spraying (black solid line) 2 mL of P1200G particles, (gray solid line) 2 mL of P800G particles, and (gray dotted line) 0.5 mL of P800G particles. For clarity, the spectra have been stacked and enlarged as indicated. (b) Photograph of the film made by spraying 0.5 mL of P800G particles under a 1W 975 nm excitation. The transparency of the film is illustrated by the presence of a blue LED placed at 8 cm on the other side of the film.

mL of P800G particles. The resulting film has an average thickness of $\sim 0.5 \mu\text{m}$. By dividing the volume of sprayed solution by 4, we increased the transparency from 16% for the 2 μm thick film to 80% for the 0.5 μm thick film.

Additional haze measurements were performed, enabling the quantification of the scattered transmission of the samples (Table 1). The film made of 0.5 mL of P800G particles presents the highest total transmission and the smallest haze, in accordance with the direct transmission measurements (Figure 5). For the films made of 2 mL of P800G or P1200G particles, the total transmission and haze are similar, but the clarity value is higher for the film made of 2 mL P1200G particles. This result can be explained by the inhomogeneous surface coverage of this film.

The UC properties of these different films are reported in Figure 6a. The film corresponding to the spray-deposition of 2 mL of P1200G particles strongly emits by UC, with an intensity difference of a factor of 12, compared to the film made of 2 mL of P800G particles, and 480, compared to the film made of 0.5 mL of P800G particles. The strong differences in terms of UC intensity should be related to the differences observed on powder samples and described in the first part of this paper. According to the evolution in Figure 1, the difference in terms of UC emission between the film made of P1200G particles and the film made of P800G particles should be of the order of 100, whereas experimentally, a value of 12 is found. This can be explained by the fact that the film made of P1200G particles is incomplete (Figure 4b). The quantity of matter that is probed by the incident light is probably less than expected, diminishing the UC signal. Between the film made of 2 mL of P800G particles (thickness = 2 μm) and the one made of 0.5 mL of P800G particles (thickness = 0.5 μm), a factor of 4 in terms of UC intensity would be expected to take into account the difference of film thickness. Experimentally, a factor of 40 is found. The difference corresponds to the increased scattering in the 2 μm thick film (Figure 5, Table 2), enhancing the incident and the emitted light pathway and leading to a strong increase of the UC.

The photograph in Figure 6b illustrates the combined properties of the 0.5 μm thick film: the high transparency, allowing the observation of an object situated at a few centimeters away from the film, and the strong up-conversion emission, which is easily detectable with the naked eye.

Table 2. Haze Measurements Performed on the Different Films Indicating Total Transmission through the Samples, Scattered Transmission, and Clarity Value

	total transmission	haze	clarity
film made of 0.5 mL P800G particles	89.3%	33.8%	97.5%
film made of 2 mL P800G particles	69.3%	97.1%	77.4%
film made of 2 mL P1200G particles	69.3%	96.6%	85.3%

CONCLUSIONS

A detailed study of the UC intensity in $\text{YVO}_4:\text{Yb},\text{Er}$ showed the necessity to anneal $\text{YVO}_4:\text{Yb},\text{Er}$ nanoparticles prepared by coprecipitation to get a high UC signal. A model based on time-resolved spectroscopy measurements enabled us to quantify the effect of the modifications of the intrinsic properties of $\text{YVO}_4:\text{Yb},\text{Er}$ upon annealing on the UC emission and gave evidence of the drastic effects of the scattering. To produce $\text{YVO}_4:\text{Yb},\text{Er}$ UC emitting coatings with controlled transparency, a trade-off should be found between high UC emission and controlled film transparency.

ASSOCIATED CONTENT

S Supporting Information

Additional spectroscopic characterizations, SEM images, and details of the calculations leading to the quantification of the scattering in the up-conversion emitting powders. This material is available free of charge via the Internet at <http://pubs.acs.org>.

AUTHOR INFORMATION

Corresponding Author

* E-mail: geraldine.dantelle@polytechnique.edu.

Present Address

[§]Institut Néel/Université Grenoble Alpes, CNRS UPR 2940, 25 Av. des Martyrs, F-38 042 Grenoble, France

Notes

The authors declare no competing financial interest.

ACKNOWLEDGMENTS

Work was partially supported by the Spanish Ministry of Economy and Competitiveness under project MAT2011-29255-C02-01. R.C.V. acknowledges her fellowship BES 2009-021748.

■ REFERENCES

- (1) Auzel, F.; Pecile, D.; Morin, D. Rare-earth doped Vitroceramics: New, Efficient, Blue and Green Emitting Materials for Infrared Upconversion. *J. Electrochem. Soc.* **1975**, *122*, 101–107.
- (2) Herbert, T.; Wannemacher, R.; Lenth, W.; Macfarlane, R. M. Blue and Green CW Upconversion Lasing in Er:YLiF₄. *Appl. Phys. Lett.* **1990**, *57*, 1727.
- (3) Scheife, H.; Huber, G.; Heumann, E.; Bar, S.; Osiac, E. Advances in Up-Conversion Lasers based on Er³⁺ and Pr³⁺. *Opt. Mater.* **2004**, *26*, 365–374.
- (4) Desirena, H.; De la Rosa, E.; Salas, P.; Meza, O. Red, Green, Blue, and White Light Upconversion Emission in Yb³⁺/Tm³⁺/Ho³⁺ Co-doped Tellurite Glasses. *J. Phys. D: Appl. Phys.* **2011**, *44*, 455308.
- (5) Chatterjee, D. K.; Rufalhah, A. J.; Zhang, Y. Upconversion Fluorescence Imaging of Cells and Small Animals using Lanthanide doped Nanocrystals. *Biomaterials* **2008**, *29*, 937–943.
- (6) Caillat, L.; Hajj, B.; Shynkar, V.; Michely, L.; Chauvat, D.; Zyss, J.; Pelle, F. Multiphoton Upconversion in Rare-Earth doped Nanocrystals for Sub-Diffractive Microscopy. *Appl. Phys. Lett.* **2013**, *102*, 143114.
- (7) Richards, B. S. Enhancing the Performance of Silicon Solar Cells via the Application of Passive Luminescence Conversion Layers. *Sol. Energy Mater. Sol. Cells* **2006**, *90*, 2329–2337.
- (8) Andriamadianana, C.; Ibanez, A.; Ferrier, A.; Joudrier, A. L.; Lombez, L.; Liotaud, M.; Guillemoles, J. F.; Pellé, F. Erbium-Doped Yttria Thin Films Prepared by Metal Organic Decomposition for Up-Conversion. *Thin Solid Films* **2013**, *537*, 42–48.
- (9) Hsu, C. W.; Zhen, B.; Qiu, W.; Shapira, O.; DeLacy, B. G.; Joannopoulos, J. D.; Soljacic, M. Transparent Displays Enabled by Resonant Nanoparticle Scattering. *Nature Comm.* **2014**, *5*, 3152.
- (10) Han, X.; Maiz, J.; Mijangos, C.; Zaldo, C. Nanopatterned PMMA-Yb:Er/Tm:Lu₂O₃ Composites with Visible Upconversion Emission. *Nanotechnology* **2014**, *25*, 205302.
- (11) Mendez-Ramos, J.; Yanes, A. C.; Santana-Alonso, A.; del-Castillo, J. Highly Efficient Up-Conversion and Bright White Light in RE Co-doped KYF₄ Nanocrystals in Sol–Gel Silica Matrix. *Chem. Phys. Lett.* **2013**, *555*, 196–201.
- (12) Chen, D. C.; Wang, Y. S.; Zheng, K. L.; Guo, T. L.; Yu, Y. L.; Huang, P. Bright Upconversion White Light Emission in Transparent Glass Ceramic Embedding Tm³⁺-Er³⁺-Yb³⁺:YF₃ Nanocrystals. *Appl. Phys. Lett.* **2007**, *91*, 251903.
- (13) Ahrens, B.; Loper, P.; Goldschmidt, J. C.; Glunz, S.; Henke, B.; Miclea, P. T.; Schweizer, S. Neodymium-Doped Fluorochlorozirconate Glasses as an Upconversion Model System for High-Efficiency Solar Cells. *Phys. Status Solidi A* **2008**, *205*, 2822–2830.
- (14) Yi, G.; Lu, H.; Zhao, S.; Ge, Y.; Yang, W.; Chen, D.; Guo, L. H. Synthesis, Characterization and Biological Application of Size-Controlled Nanocrystalline NaYF₄:Yb,Er Infrared-to-Visible Up-Conversion Phosphors. *Nano Lett.* **2004**, *4*, 2191–2196.
- (15) Mialon, G.; Türkcan, S.; Dantelle, G.; Collins, D.; Hadjipanayi, M.; Taylor, R. A.; Gacoin, T.; Alexandrou, A.; Boilot, J. P. High Up-Conversion Efficiency of YVO₄:Yb,Er Nanoparticles in Water down to the Single-Particle Level. *J. Phys. Chem. C* **2010**, *114*, 22449–22454.
- (16) Calderón-Villajos, R.; Zaldo, C.; Cascales, C. Enhanced Upconversion Multicolor and White Light Luminescence in SiO₂-Coated Lanthanide-Doped GdVO₄ Hydrothermal Nanocrystals. *Nanotechnology* **2012**, *23*, 505205.
- (17) Lu, Q.; Guo, F. Y.; Sun, L.; Li, A. H.; Zhao, L. C. Silica/Titania-Coated Y₂O₃:Tm³⁺, Yb³⁺ Nanoparticles with Improvement in Upconversion Luminescence induced by Different Thickness Shells. *J. Appl. Phys.* **2008**, *103*, 123533.
- (18) Shao, W.; Chen, G. Y.; Damasco, J.; Wang, X. L.; Kachynski, A.; Ohulchanskyy, T. Y.; Yang, C. H.; Agren, H.; Prasad, P. N. Enhanced Upconversion Emission in Colloidal (NaYF₄:Er³⁺)/NaYF₄ Core/Shell Nanoparticles Excited at 1523 nm. *Opt. Lett.* **2014**, *39*, 1386–1389.
- (19) Yin, W.; Zhou, L.; Gu, Z.; Tian, G.; Jin, S.; Yan, L.; Liu, X.; Xing, G.; Ren, W.; Liu, F.; Pan, Z.; Zhao, Y. Lanthanide-Doped GdVO₄ Upconversion Nanophosphors with Tunable Emissions and their Applications for Biomedical Imaging. *J. Mater. Chem.* **2012**, *22*, 6974–6981.
- (20) Maurin, I.; Dantelle, G.; Boilot, J. P.; Gacoin, T. A Protected Annealing Process for the Production of High Quality Colloidal Oxide Nanoparticles with Optimized Physical Properties. *J. Mater. Chem. C* **2013**, *1*, 13–22.
- (21) Bubb, D. M.; Cohen, D.; Qadri, S. B. Infrared-to-Visible Upconversion in Thin Films of LaEr(MoO₄)₃. *Appl. Phys. Lett.* **2005**, *87*, 131909.
- (22) Mialon, G.; Gohin, M.; Gacoin, T.; Boilot, J. P. High-Temperature Strategy for Oxide Nanoparticle Synthesis. *ACS Nano* **2008**, *2*, 2505–2512.
- (23) Fleury, B.; Dantelle, G.; Darbe, S.; Boilot, J. P.; Gacoin, T. Transparent Coatings made from Spray-Deposited Colloidal Suspensions. *Langmuir* **2012**, *28*, 7639–7645.
- (24) Wang, X.; Kong, X.; Shan, G.; Yu, Y.; Sun, Y.; Feng, L.; Chao, K.; Lu, S.; Li, Y. Luminescence Spectroscopy and Visible Upconversion Properties of Er³⁺ in ZnO nanocrystals. *J. Phys. Chem. B* **2004**, *108*, 18408–18413.
- (25) Wang, H.; Yu, M.; Lin, C. K.; Lin, J. Core-Shell structured SiO₂@YVO₄:Dy³⁺/Sm³⁺ Phosphor Particles: Sol–Gel Preparation and Characterization. *J. Colloid Interface Sci.* **2006**, *300*, 176–182.
- (26) Meltzer, R. S.; Feofilov, S. P.; Tissue, B.; Yuan, H. B. Dependence of Fluorescence Lifetimes of Y₂O₃:Eu Nanoparticles on the Surrounding Medium. *Phys. Rev. B* **1999**, *60*, R14012.
- (27) Vetrone, F.; Boyer, J. C.; Capobianco, J. A.; Speghini, A.; Bettinelli, M. NIR to Visible Upconversion in Nanocrystalline and Bulk Lu₂O₃:Er³⁺. *J. Phys. Chem. B* **2002**, *106*, 5622–5628.
- (28) Mialon, G.; Türkcan, S.; Alexandrou, A.; Gacoin, T.; Boilot, J. P. New Insights into Size Effects in Luminescent Oxide Nanocrystals. *J. Phys. Chem. C* **2009**, *113*, 18699–18706.
- (29) Dantelle, G.; Fleury, B.; Boilot, J. P.; Gacoin, T. How to Prepare the Brightest Luminescent Coatings? *ACS Appl. Mater. Interfaces* **2013**, *5*, 11315–11320.
- (30) Li, H.; Xu, C. T.; Lindgren, D.; Xie, H.; Thomas, D.; Gundlach, C.; Andersson-Engels, S. Balancing Power Density based Quantum Yield Characterization of Upconverting Nanoparticles for Arbitrary Excitation Intensities. *Nanoscale* **2013**, *5*, 4770–4775.
- (31) Dyck, N. C.; van Veggel, F. C. J. M.; Demopoulos, G. P. Size-Dependent Maximization of Up-Conversion Efficiency of Citrate-Stabilized β-phase NaYF₄:Yb³⁺,Er³⁺ Crystals via Annealing. *ACS Appl. Mater. Interfaces* **2013**, *5*, 11661–11667.